ผลของการแทนที่ La ด้วย Sr และ Gd ในสารประกอบเพอรอฟสไกต์ $La_{1-x-y}Sr_xGd_yMnO_3$ ที่มีต่อโครงสร้างและสมบัติทางแม่เหล็ก

Influence of La substitutions with Sr and Gd in $La_{1-x-y}Sr_xGd_yMnO_3$ perovskite compound on structure and magnetic properties

Saowalak Saengplot[1], Sujittra Daengsakul[1,2,*], Adulphan Pimsawat[1] and Santi Maensiri[3]

[1]Department of Physics, Faculty of Science, Khon Kaen University, Khon Kaen 40002, Thailand

[2]The Integrated Nanotechnology Research Center, Khon Kaen University, Khon Kaen 40002, Thailand

[3]School of Physics, Institute of Science, Suranaree University of Technology, Nakhon Ratchasima, 30000, Thailand

[*]Corresponding author email sujdaeng@gmail.com

บทคัดย่อ

งานวิจัยนี้ได้ทำการศึกษาโครงสร้างผลึก ลักษณะสัณฐานวิทยา และสมบัติทางแม่เหล็กของสารประกอบแมงกาไนต์โครงสร้างแบบเพอรอฟสไกต์ของ $La_{1-x-y}Sr_xGd_yMnO_3$ (LSGM) ซึ่งกำหนดให้มีการแทนที่ของทั้ง Sr และ Gd ในตำแหน่งของ La (หรือตำแหน่ง A-site) ในปริมาณที่ทำให้สารตัวอย่างทุกตัว มีค่า $\langle r_A \rangle$ หรือค่าขนาดรัศมีไอออนเฉลี่ยที่อยู่ในตำแหน่ง A-site คงที่อยู่ที่ ~1.24 Å โดยที่ผลของปริมาณ Mn^{4+} และค่าความไม่สอดคล้องกันของขนาดไอออนที่ตำแหน่ง A-site (หรือ σ^2) ที่เปลี่ยนแปลงตามปริมาณการแทนที่นี้เป็นตัวแปรสำคัญที่ถูกนำไปพิจารณา สารตัวอย่างผงอนุภาคนาโน LSGM ถูกเตรียมด้วยวิธีการสลายตัวทางความร้อนโดยใช้น้ำที่อุณหภูมิ 900 °C เป็นเวลา 6 ชั่วโมง ก่อนนำไปศึกษาวิเคราะห์ด้วยเทคนิค SEM, TEM, XRD และ VSM ผลจากเทคนิค XRD แสดงให้เห็นว่าทุกสารตัวอย่างมีโครงสร้างเพอร์รอฟสไกต์ที่มีโครงสร้างผลึกแบบรอมโบฮีดรอล ผลการตรวจสอบลักษณะสัณฐานวิทยาจากภาพถ่าย SEM และ TEM พบว่าอนุภาคที่เตรียมได้มีขนาดเฉลี่ยอยู่ในช่วง 28 – 40 nm และมีลักษณะเป็นทรงกลมเกาะกลุ่มรวมกัน ผลทางแม่เหล็กพบว่าทุกสารตัวอย่างแสดงพฤติกรรมความเป็นแม่เหล็กเฟอร์โรแบบอ่อนๆ ทั้งนี้การเพิ่มขึ้นของปริมาณไอออน Mn^{4+} และค่า σ^2 ส่งผลให้ขนาดอนุภาค แมกนีไตเซชัน (M) และอุณหภูมิคูรี (T_C) มีค่าลดลงอย่างมาก เนื่องจากการเพิ่มชั้นสารแม่เหล็ก Gd เข้าไปในโครงสร้าง และการเพิ่มสูงขึ้นของค่า σ^2 จะส่งผลต่อพฤติกรรมการจัดเรียงตัวของสปินในโครงสร้าง และทำให้ไอออน Mn^{3+} และ Mn^{4+} มีการจัดเรียงตัวเป็นไปแบบสุ่ม ซึ่งเป็นการทำลายความระเบียบของโครงสร้างที่มีการจัดเรียงตัวแบบเฟอร์โร

ที่เป็นสายยาวให้กลายเป็นการจัดเรียงตัวกันเป็นกลุ่มสั้นๆ จนเกิดเป็นสถานะแม่เหล็กในรูปแบบของ spin-cluster glass

ABSTRACT

This research reports the studies of crystallographic structure, morphology and magnetic properties of a manganite compound which substitution of Gd and Sr ions at La (or A-site) in the perovskite structure of $La_{1-x-y}Sr_xGd_yMnO_3$ (LSGM). While the quantity of Gd and Sr given gives the average size of the cations occupying in A-site or ($\langle r_A \rangle$) is fixed at ~1.24 Å for all samples, the significant parameters of Mn^{4+}content and the size mismatch of A-site cations (σ^2) changed from the substitution of Gd and Sr for La is focused. The LSGM nanopowders are prepared by using the thermal hydro-decomposition method at 900°C in air for 6 h. The influence of Gd and Sr substitution for La in the sample was characterized by XRD, SEM, TEM and VSM techniques. The XRD result shows that all the prepared samples indexed to a single rhombohedral phase. The morphological investigation of the powder samples from SEM and TEM images reveals the spherical nanoparticles shape with an agglomeration. The average particle sizes of prepared samples are in the range of 28 – 40 nm. The magnetic measurement shows soft ferromagnetic behavior of all samples. The increasing of Mn^{4+} contents and σ^2 value (or Gd content) decreases particle size (D), magnetization (M) and Curie temperature (T_C) strongly. A large σ^2, and an introduction of magnetic layers result in a random arrangement of spin-ordering and also destroy the coupling of Mn^{3+} and Mn^{4+} ions in the long-range FM ordering into the short-range magnetically ordered clusters and form spin-cluster glass state.

คำสำคัญ: แมงกาไนต์ อนุภาคนาโนแม่เหล็ก อุณหภูมิคูรี แมกนีโตเซชัน

Keywords: Manganite, Magnetic nanoparticles, Curie temperature, Magnetization

INTRODUCTION

The hole-doped manganite perovskites $A_{1-x}B_xMnO_3$ (A = La, Ln, Pr and B = alkaline earth elements) have attracted considerable interest because of their intriguing magnetic and electrical properties such as paramagnetic to ferromagnetic (FM-PM) transition, insulator to metal (I-M) transition and colossal magnetoresistance (Reshmi et al., 2013; Shinde et al., 2012; Krishna et al., 2009; Revzin et al., 2000). These exceptional perov-skites are contemporarily recognized in various fields of applications, for examples, magnetic sensors, magnetic resistance device, infrared devices, fuel cells, magnetic refrigeration and read heads (Maity

et al., 2013; Chen et al 2011; Cheikh-Rouhou Koubaa et al., 2007). Typically, for manganite perovskites compound, when some trivalent ions (i.e. La^{3+}) are substituted divalent cations such as Sr^{2+}, a compound of $La^{3+}_{1-x}Sr^{2+}_{x}Mn^{3+}_{1-x}Mn^{4+}_{x}O_3$ or LSM will be obtained. This substitution causes a creation of holes (hole-doping) that consequently induces a mixed valence state of Mn ions (Mn^{3+}/Mn^{4+}) that leads to the enhancement of the magnetic transition temperature and the occurrence of the ferromagnetism and conductivity in this compound (Goodenough, 1955; Verelest et al., 1993). Amongst various manganite compounds, strontium-doped manganite (LSM) is attractive because of its large magnetic moment, high paramagnetic-ferromagnetic transition temperature (T_C) and metal-insulator transition temperature (T_{MI}) (Zi et al., 2009).

In order to elucidate the aforementioned phenomena of manganite compounds, there have been numerous attempts to investigate their magnetic properties when varying the Mn^{4+} content, average size of the cations occupying in A-site, $\langle r_A \rangle$ and the mismatch factor (σ^2) originated from the disorder of ionic size in A-site (Raveau et al., 1998; Asamitsu et al., 1996; Gaudon et al., 2002; Dhahri et al., 2008). Previous studies have revealed that the Mn^{4+} content, the values of $\langle r_A \rangle$ and σ^2 have notable influences on the crystal structure, magnetic and CMR properties of LSMs. Moreover, we have proposed that the average Mn oxidation state in $La_{1-x}Sr_xMnO_3$ ($0 \le x \le 0.5$) can be modulated by the variation of $\langle r_A \rangle$ and σ^2 (Daengsakul et al., 2012; Daengsakul et al., 2009). The magnetization (M) is dramatically increased with respect to the increased $\langle r_A \rangle$ of until $\langle r_A \rangle$ reaches ~ 1.244 Å at which M becomes the highest (Daengsakul et al., 2012). Our finding agrees with the previous work that the Curie temperature (T_C) is highest when $\langle r_A \rangle$ is in the range of 1.23–1.26 Å (Rao, et al., 1997). Although, the effect of $\langle r_A \rangle$ on T_C has been studied, the comprehensive explanation of this point remains absent. Moreover, the investigations of the other crucial effects (such as Mn^{4+} content or doping with magnetic ions) under the fixed $\langle r_A \rangle$ values have not been reported. Therefore, in order to unravel these effects on magnetic properties, we have studied in a $La_{1-x-y}Sr_xGd_yMnO_3$ (LSGM) series in which a nonmagnetic ion La^{3+} is partially replaced by magnetic ion of Gd^{3+} at fixed $\langle r_A \rangle$ ~1.24 Å while the Mn^{3+}/Mn^{4+} ratio are systematically increased by Sr doping. The studied LSGM samples are synthesized as nano-particle by using the thermal hydro-decomposition method (Daengsakul et al., 2009). The influence of introducing magnetic layer and hole concentration (or Mn^{4+}

content) on their structure and magnetic properties are examined by the XRD, SEM, TEM and VSM techniques, respectively.

RESEARCH METHODOLOGY

In this work, we have studied $La_{1-x-y}Sr_xGd_yMnO_3$ (LSGM) compounds. In order to keep constant $\langle r_A \rangle$ at ~1.24 Å for each sample, the concentrations of Gd and Sr were increased together (i.e., introducing both magnetic ions and hole concentration simultaneously). For this case, the mismatch factor σ^2 increases from 1.954 - 6.159 (x 10^{-3} Å^2) with the increase of Gd (or Sr) doping from 0-20% ($0 \le x \le 0.45$ และ $0 \le y \le 0.2$). All LSGM samples were synthesized by the thermal-hydro decomposition method (Daengsakul et al., 2009). The samples were prepared by mixing 99.99% purity powders of La, Sr, Mn and Gd acetate salts and dissolved in distilled water. Afterwards, the solution was thermally decomposed in an oven at 900 °C under air atmosphere for 6 h and it was subsequently cooled down to room temperature before being ground to yield nanopowders. The variation of theoretical values of Mn^{4+} content is assembled in Table 1, while the variation of σ^2 with the doping level of Gd is rendered in Fig. 1. The theoretical values of $\langle r_A \rangle$ and σ^2 are calculated from Equations (1) and (2), respectively.

The ionic radii of related cations are obtained from Shannon ($r_{La^{3+}}$ = 1.216 Å, $r_{Gd^{3+}}$ = 1.107 Å, $r_{Sr^{2+}}$ = 1.31 Å) (Shannon, 1976) for the nine-fold coordination of A cations, as proposed by Rodriguez-Martinez and Paul Attfield (Rodriguez-Martinez and Attfield, 1998). These radii correspond well to those of a distorted perovskite lattice.

Table 1 The theoretical content values of Sr, Gd, Mn^{4+}, $\langle r_A \rangle$ and σ^2 for all studied LSGM nanopowder samples.

Composition Formula	Abbreviation	content		%Mn^{4+}	$\langle r_A \rangle$ (Å)	σ^2 (10^{-3} Å^2)
		Sr (x)	Gd (y)			
$La_{0.67}Sr_{0.33}MnO_3$	LSM	0.33	0	33%	1.2470	1.954
$La_{0.62}Sr_{0.33}Gd_{0.05}MnO_3$	LSG05M	0.33	0.05	33%	1.2416	2.856
$La_{0.51}Sr_{0.39}Gd_{0.10}MnO_3$	LSG10M	0.39	0.10	39%	1.2418	3.971
$La_{0.4}Sr_{0.45}Gd_{0.15}MnO_3$	LSG15M	0.45	0.15	45%	1.2419	5.085
$La_{0.3}$ $Sr_{0.50}Gd_{0.20}MnO_3$	LSG20M	0.50	0.20	50%	1.2412	6.159

$$\langle r_A \rangle = (1 - \mathrm{x} - \mathrm{y}) r_{\mathrm{La}^{3+}} + (\mathrm{x}) r_{\mathrm{Sr}^{2+}} + (\mathrm{y}) r_{\mathrm{Gd}^{3+}} \quad (1)$$

$$\sigma^2 = \sum x_i r_i^2 - \langle r_A \rangle^2 = [(1 - \mathrm{x} - \mathrm{y}) r_{\mathrm{La}^{3+}}^2 + (\mathrm{x}) r_{\mathrm{Sr}^{2+}}^2 + (\mathrm{y}) r_{\mathrm{Gd}^{3+}}^2] - \langle r_A \rangle^2 \quad (2)$$

$$La_{1-x-y}Sr_xGd_yMnO_3 \rightarrow La^{3+}_{1-x-y}Sr^{2+}_xGd^{3+}_yMn^{3+}_{1-x-y}Mn^{4+}_xO^{2-}_3 \quad (3)$$

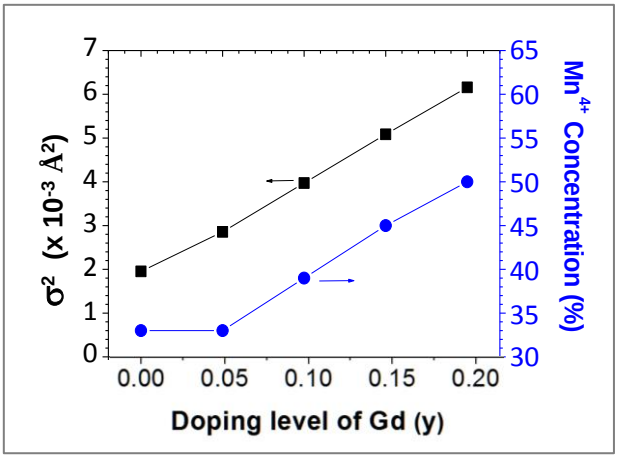

Fig. 1. The theoretical content values of Gd, Mn^{4+} and σ^2 for all studied LSGM nanopowder

In this article, the crystal structure and phase purity of the LSGM nanopowders were characterized by X-ray diffraction (XRD) using a Philips PW 3040 X-ray diffractometer with CuK**α** radiation, and the average crystallite sizes were calculated by Debye Scherrer's formula. The morphology of the prepared samples was revealed by using a scanning electron microscope (SEM) (LEO 1450VP, UK). The morphology, size distribution and particle size of LSGM samples were observed by a transmission electron microscope (TEM) (JEOL 2010, Japan) at an accelerating voltage of 200 kV. The magnetic hysteresis loops were measured by a vibrating sample magneto-meter (VSM) (Quantum Design VersaLab, USA) at room temperature in the applied field range 30 kOe. The temperature-dependences of magnetization were also measured using the VSM in the temperature range of 50-390 K in both zero field cooled (ZFC) and field cooled (FC) condition. The sample was cooled from room temperature to 50 K at zero magnetic field and then magnetization (M_{ZFC}) was measured as the sample was warmed under applying a magnetic field of 100 Oe. In the field cooled case, the sample was cooled from room temperature to 50 K under a magnetic field of 30 kOe, and then magnetization (M_{FC}) measured at elevated temperature in the presence of a magnetic field of 100 Oe. The

Curie temperature (T_C) defined by the maximum of |dM/dT| from M-T curve.

RESULTS AND DISCUSSION

Fig. 2 depicts the X-ray diffraction patterns of the $La_{1-x-y}Sr_xGd_yMnO_3$ nanopowder. The XRD data of all the samples were analyzed by the Rietveld refinement method. It is found that all the samples can be indexed to the single rhombohedral phase with $R\bar{3}C$ space group. The diffraction peaks shift to a higher degree with increasing Gd concentration (y) as shown inset in Fig. 2**.** This indicates a decrease in lattice parameter and unit cell volume (*V*). The variations in the lattice size, the average bond length of Mn-O, $\langle d_{Mn-O} \rangle$, and the average Mn-O-Mn bond angle, $\langle \theta_{Mn-O-Mn} \rangle$, for all samples are compiled in Table 2. It is evident that *V* and $\langle d_{Mn-O} \rangle$ decrease with increasing Gd content while the $\langle \theta_{Mn-O-Mn} \rangle$ remains constant for all samples. Although the introduction Gd, which is a smaller ion than La, into the LSGM perovskite is expected to produce a deformation of the octahedral MnO_6, but constant $\langle r_A \rangle$ results in the variation of Mn-O bond length.

The average crystalline sizes (D) are approximated by X-ray line broadening method using Debye Scherrer's formula ($D_{XRD} = \frac{k\lambda}{\beta \cos\theta}$), where β is the full width at half-maximum (FWHM) value, λ is the wavelength of X-ray (1.54056 Å), *k* is the shape factor (Suryanarayana and Grant, 1998). The obtained average crystalline sizes of LSGM samples are in the range of 17.8– 22.5 nm and these sizes decrease with increasing Gd and Mn^{4+} ions content as shown in Fig. 3. The decrease of the unit cell volume, $\langle d_{Mn-O} \rangle$ value and crystalline size is attributed to the substitution of Gd, which has smaller ionic radius than La. Furthermore, the increase of a smaller radii size of Mn^{4+} ions ($r_{Mn^{4+}}$ = 0.530 Å) than that of Mn^{3+} ions ($r_{Mn^{4+}}$ = 0.645 Å) taking place along with Gd doping also causes the shrinkage of the unit cell volume, $\langle d_{Mn-O} \rangle$ value and crystalline size.

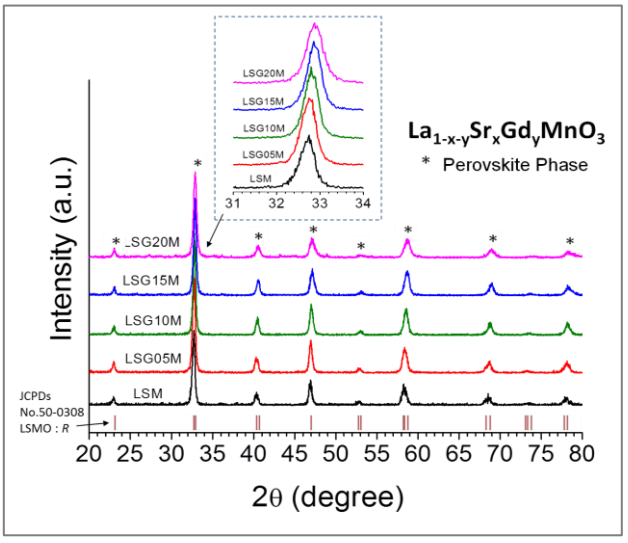

Fig. 2 XRD patterns of LSGM nanopowders.

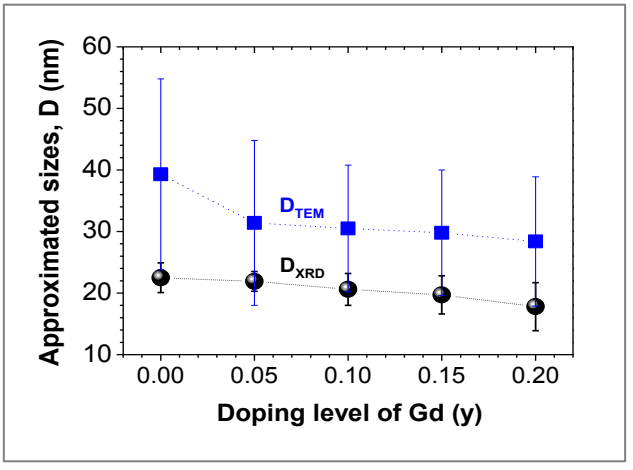

Fig. 3 The relationship between the approximated sizes of the LSGM nanopowder sample obtained from X-ray line broadening method and histogram of the size distribution from TEM image.

The morphology of the LGSM samples investigated by SEM and TEM techniques (for only LGSM samples with y = 0, 0.1 and 0.20) are presented in Figs. 4–5. The SEM images (Fig. 4) reveal that the prepared LGSM samples are made up of spherical nanoparticles with agglomeration of particles in the submicron range. While the TEM images shown in Fig. 5 reveal an abundance of nearly spherical particles. As seen in the histogram of the size distribution, we find that the average particles size (D_{TEM}) are in the range of 28.4 – 39.3 nm, which is slightly larger than those obtained from XRD result (see Fig. 3). This is

because the crystallite size derived from X-ray line broadening method does not have the actual full width at half-maximum (FWHM) value of Debye Scherrer's formula.

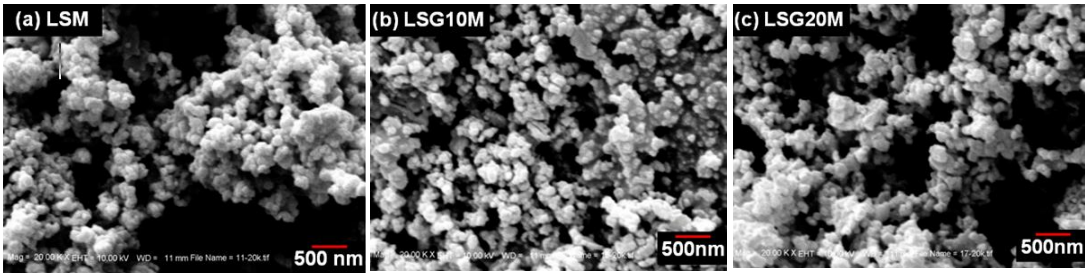

Fig. 4 SEM micrographs of the LSGM nanoparticle: (a) LSM, (b) LSG10M and (c) LSG20M.

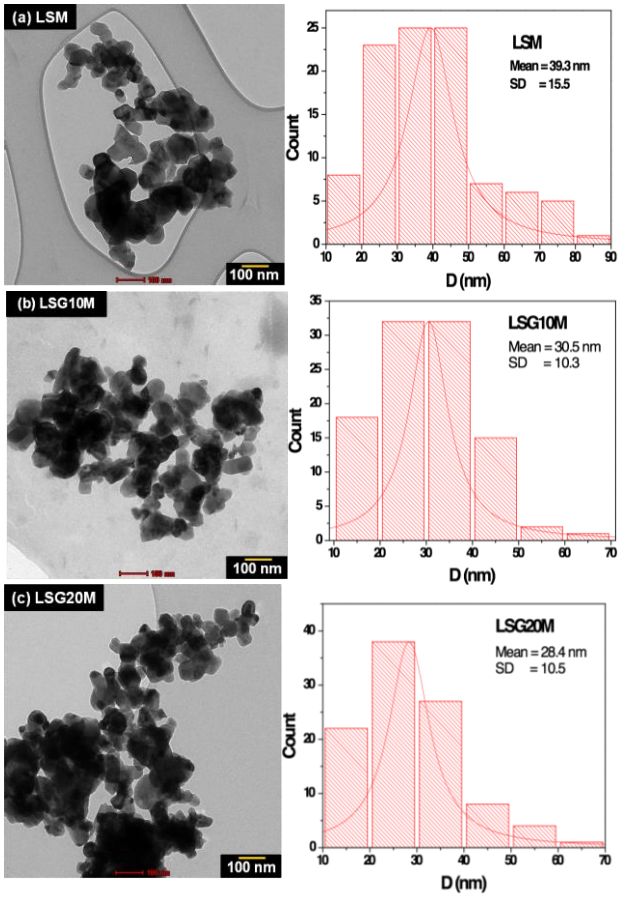

Fig. 5 TEM micrographs and histogram of the size distribution of the LSGM nanoparticle: (a) LSM, (b) LSG10M and (c) LSG20M.

The magnetic field dependence magnetization measured at 300 K (room temp.) in the magnetic field strength up to 30,000 Oe is shown in Fig. 6. It is apparent that all the samples show the soft ferromagnetic behavior with a small hysteresis loop at room temperature (coercive field < 50 Oe). The FM-PM transition temperature or T_C for all LSGM samples is evaluated from the temperature-dependence of magnetization which shown in Fig. 7 (T_C defined as the temperature where the slope, |dM/dT|, reaches a maximum value calculated from the ZFC curve (Kao et al., 2007). The values of magnetization and T_C for all samples as a function of three parameters i.e., (i) the doping level of Gd, (ii) the mismatch effect factor or σ^2 and (iii) the theoretical concentration of Mn^{4+} ions are listed table 2. These findings indicate that the M and T_C decreases strongly with respect to the increase these three parameters. From Fig. 8, we find that the decreasing of the highest values of M = 52.1 emu/g and T_C = 365 K belongs to the LSM sample which no doping with Gd to the lowest values of M = 12.3 emu/g and T_C = 266 K for LSG20M sample. This result suggests that the fixing $\langle r_A \rangle$ at ~1.24 Å cannot enhance M and T_C. This indicates that the Mn^{4+} content and σ^2 are the important parameters that contribute greatly to the value of T_C and magnetic property. Moreover, the substitution of magnetic Gd ion to La-site in manganite structure cannot enhance ferromagnetic behavior, but it inhibits the long-range order of existing FM, leading to lower M and T_C.

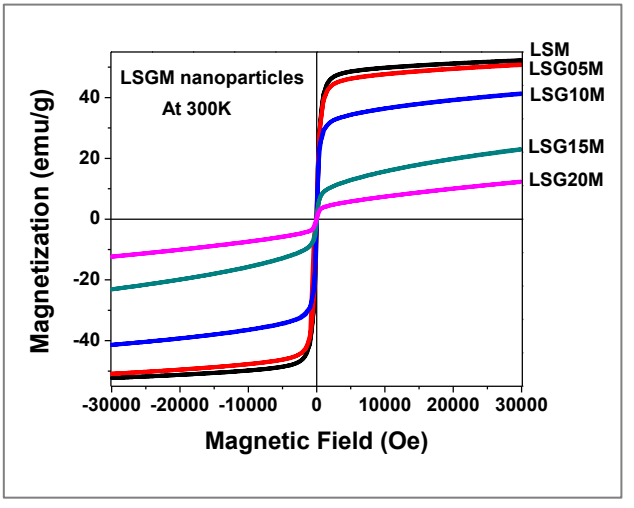

Fig. 6 M-H curves of LSGM nanopowders measured at 300K in field up 3T

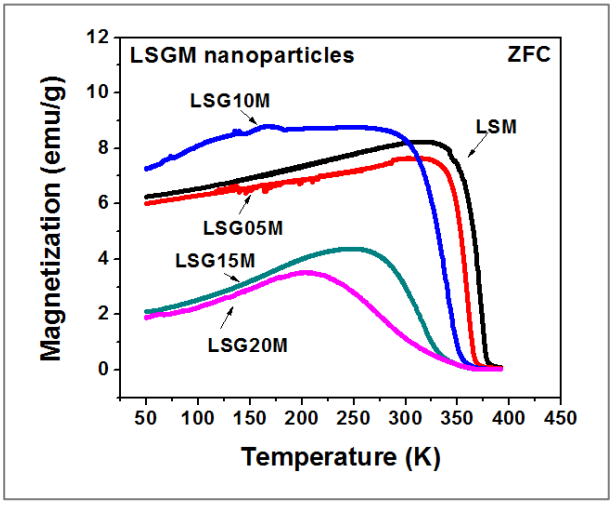

Fig. 7 Temperature dependence of the zero-field cooling magnetization curves for all LSGM nanoparticles measured at 50–390 K.

The decrease in M with increasing Gd content agrees with the reported findings (Kao et al., 2007; Qixiang et al., 2008; Ling et al, 2008). This is because the substitution of Gd ions interrupts La-O-La(Sr) layers causing Mn-O-Mn not to form homogeneous long-range order. Instead, Mn-O-Mn are clustered to form spin-cluster glass state (Qixiang et al., 2008; Ling et al., 2008; Liang et al., 2013). This explanation is confirmed by the splitting of ZFC and FC magnetization curves at low temperature as shown in Fig. 9.

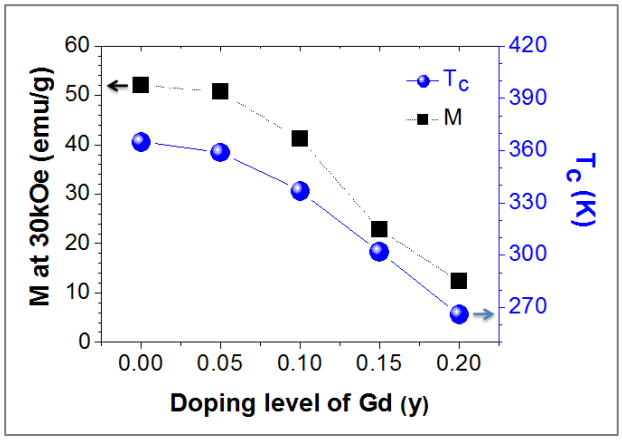

Fig. 8 The variation of M (measured at H ~ 30kOe) and T_C of the LSGM nanopowders with the doping level of Gd.

In order to investigate the short (or long)-range spin order and magnetic behavior for the LSGM samples, the ZFC and FC magnetization curves in a low field of 100 Oe in the temperature range 50–390 K are measured and then presented in Fig. 9. It can be seen that the PM–FM phase transition is broadened by the increase Gd content, and T_C moves to the lower temperature likely because the increase magnetization curves for all LSGM nanopowders of Gd substitution yields large magnetic moment. Consequently, the antiferromagnetic phenomenon appears in low temperature range. This is because the magnetism of Mn-O-Mn is strengthened with decreasing temperature, and the induction of Mn-O-Mn magnetism causes Gd to transform gradually from a random arrangement to the orderly arrangement of Gd-O-Gd chains. Hence, the antiferromagnetic arrangement between Mn-O-Mn and Gd-O-Gd forms on the low temperature range (Kao et al., 2007). Moreover, as seen in Fig. 9, the FC magnetization below T_C for all samples does not become saturated but it rapidly increases with temperature cooling. This indicates that the magnetic ordering of rare earth ions at A-site occurs at lower temperature.

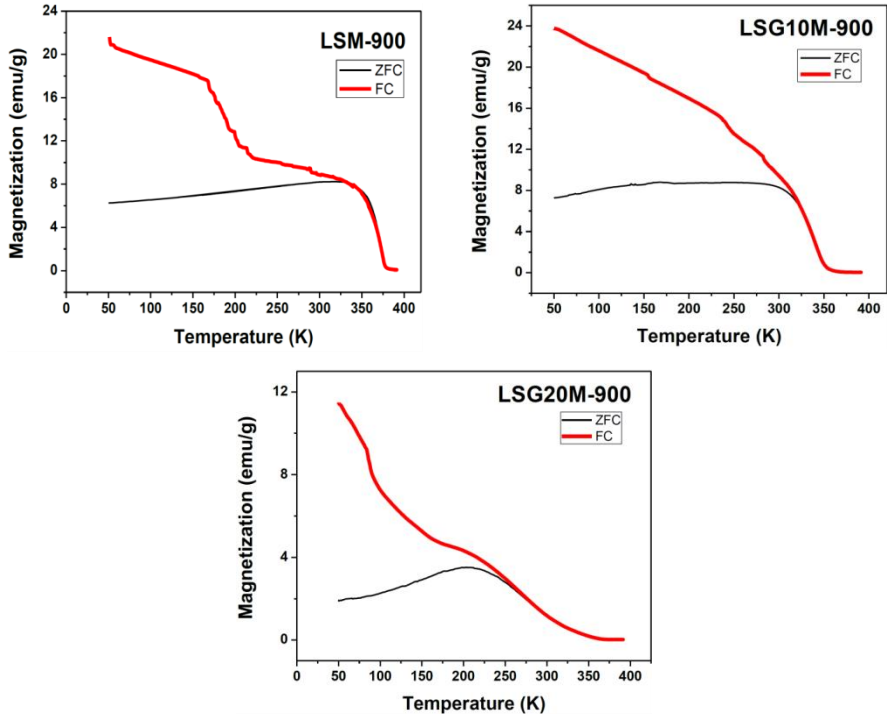

Fig. 9 Temperature dependence of the zero-field cooling and field cooling (under H = 100 Oe)

Table 2 Structural parameters and related values of LSGM nanopowder samples (R: Rhombohedral phase).

Samples	LSM	LSG05M	LSG10M	LSG15M	LSG20M
Crystal structure	R	R	R	R	R
V (Å^3)	348.4	347.0	345.9	343.9	343.4
$\langle d_{Mn-O} \rangle$ (Å)	1.950	1.939	1.936	1.926	1.925
$\langle \theta_{Mn-O-Mn} \rangle$ (°)	167.5	166.2	166.1	166.2	166.3
D_{XRD} (nm)	22.5±2.4	21.9±1.6	20.6±2.6	19.7±3.1	17.8±3.9
D_{TEM} (nm)	39.3	31.4±13.4	30.5±10.3	29.8±10.2	28.4±10.5
M *at 30kOe* (emu/g)	52.1	50.7	41.2	22.9	12.3

CONCLUSION

A series of $La_{1-x-y}Sr_xGd_yMnO_3$ nano-powders with fixing $\langle r_A \rangle$ at ~1.24 Å were prepared by the thermal hydro-decomposition method. The structural characterization of all samples shows the single rhombohedral phase with $R\bar{3}C$ space group. The increase of Gd content in the sample affects the average particle size and the unit cell volume decrease. It is because of the substitution of Gd to La-site leads to lattice distortion. For the magnetic properties, M and T_C decrease with increasing Gd content. This result can be explained by the increase of the magnetic moment of Gd causing the formation of Mn-O-Mn cluster and spin-cluster glass state.

ACKNOWLEDGEMENT

The authors would like to acknowledge the Department of Physics, Khon Kaen University for providing XRD, SEM, TEM and VSM facilities. This work was supported by the Thailand Research Fund (TRF MRG5580033), The Integrated Nanotechnology Research Center, Khon Kaen University and the Nanotechnology Center (NANOTEC), NSTDA, Ministry of Science and Technology, Thailand, through its program of Center of Excellence Network on Advanced Nanomaterials for Energy Production and Storage.

REFERENCES

Reshmi, C.P., Savitha Pillai, S., Suresh, K.G. and Manoj Raama. (2013). Room temperature magnetocaloric proper-ties of Ni substituted $La_{0.67}Sr_{0.33}MnO_3$. J. Solid State Sci. 19: 130-135.

Shinde, K.P., Pawar, S.S., Shirage, P.M. and Pawar, S.H. (2012). Studies on mor-phological and magnetic properties of $La_{1-x}Sr_xMnO_3$. J. Appl. Surf. Sci. 258: 7417-7420.

Krishna, D.C. and Venugopal Reddy, P. (2009). Magnetic transport behavior of nano-crystalline $Pr_{0.67}A_{0.33}MnO_3$ (A= Ca, Sr, Pb and Ba) manganites. J. Alloys Compd. 479(1-2): 661-669.

Revzin, B., Rozenberg, E., Gorodetsky, G., Pelleg, J. and Felner, I. (2000). Magnetization and Magnetoresistance of Magnetically Soft Manganite $La_{0.67}Sn_{0.33}MnO_3$. J. Magn. Mater. 204: 215-216.

Maity, S., Ray, S.K. and Bhattacharya, D. (2013). Phase, morphology and core-level electron spectroscopy of nano-sized $La_{0.65}Sr_{0.35}MnO_3$ powders pre-pared by solution combustion synthesis. J. Phys. & Chem. Solids. 74: 315-321.

Chen, G.Y., Zhu. J., Zhang, S., Dong, X., Lei, X., Tang, X., Wang, G. and Jiang, J. (2011). Preparation and Characterization of Lanthanum Strontium Manganite Thin Films by Metal-Organic Chemical Liquid Deposition. J. Am. Ceram. Soc. 94(9): 2783-2787.

Cheikh-Rouhou Koubaa, W. Koubaa, M. and Cheikh-Rouhou, A. (2007). Effects of silver doping upon the physical properties of $La_{0.7}Sr_{0.3-x}Ag_xMnO_3$ manganese oxide. J. Magn. Mater. 316(2): e648-651.

Goodenough, J.B. (1955). Theory of the role of covalence in the perovskite-type manganites [La, M(II)]MnO_3. Phys. Rev. 100(2): 564–573.

Verelest, M., Rangavittal, N., Rao, C.N.R. and Rousset, A. (1993). Metal-insulator transitions in anion excess $LaMnO_{3+\delta}$ controlled by the Mn^{4+} content. J. Solid State Chem. 104: 74-80.

Zi, Z.F., Sun, Y.P., Zhu, X.B., Hao, C.Y., Luo, X., Yang, Z.R., Dai, J.M. and Song, W.H. (2009). Electrical transport and magnetic properties in $La_{0.7}Sr_{0.3}MnO_3$ and $SrFe_{12}O_{19}$ composite system. J. Alloys Comp. 477: 414-419.

Raveau, B., Maignan, A., Martin, C. and Hervieu, M. (1998). Colossal Magnetoresistance Manganite Perovskites: Relations between Crystal Chemistry and Properties. Chem. Mater. 10(10): 2641-2652.

Asamitsu, A., Morimoto, Y., Kumai, R., Tomioka, Y., and Tokura, Y. (1996). Magneto-structural phase transitions in $La_{1-X}Sr_XMnO_3$ with controlled carrier density. Phys. Rev. B 54(3): 1716-1723.

Gaudon, M., Laberty-Robert, C., Ansart, F., Stevens, P. and Rousset, A. (2002). Preparation and characterization of $La_{1-x}Sr_xMnO_{3+\delta}$ ($0 \le x \le 0.6$) powder by sol–gel processing. Solid State Sci. 4: 125-133.

Dhahri, A., Dhahri, J., Zemnib, S., Oumezzine, M., Said, M. and Vincent, H. (2008). Synthesis, structural, magnetic and electrical properties of $La_{1-x}Cd_xMnO_3$ manganites ($0.1 \le x \le 0.5$). J. Alloy. Comp. 450(1-2): 12-17.

Daengsakul, S., Thomas, C., Mongkolkachit, C. and Maensiri, S. (2012). Effects of crystallite size on magnetic properties of thermal-hydro decomposition prepared $La_{1-x}Sr_xMnO_3$ nanocrystalline powders. Solid State Sci. 14: 1306-1014.

Daengsakul, S., Mongkolkachit, C., Thomas, C., Siri, S., Thomas, I., Amornkitbamrung, V. and Maensiri, S. (2009). A simple thermal decomposition synthesis, magnetic properties, and cytotoxicity of $La_{0.7}Sr_{0.3}MnO_3$ nanoparticles. Appl. Phys. A 96: 691-699.

Rao, C. N. R. and Mahesh, R. (1997). Giant magnetoresistance in manganese oxides. Solid State Mater. Sci. 2: 32-39.

Shannon, R.D. (1976). Crystal Physics, Diffraction. Theoretical and General Crystallography. Acta. Crystallogr., Sect A: Cryst. Phys. Diffr., Theor. Gen, Crystallogr., 32: 751-767.

Rodriguez-Martinez, L.M. and Attfield, J.P. (1998). Cation disorder and the metal-insulator transition temperature in manganese oxide perovskites. Phys. Rev. B 58: 2426-2429.

Suryanarayana, C. and Grant, N.M. (1998). X-ray Diffraction: A Practical Approach. Plenum Press, USA. pp.134-149.

Kao, M.C., Chen, H.Z., Young, S.L., Shen, C.Y. and Horng, L. (2007). Synthesis characterization of magnetic properties in $La_{0.7-x}Ln_xPb_{0.3}MnO_3$ (Ln = Pr, Nd, Gd, Dy, Sm and Y) perovskite compounds. J. Alloys Compd. 440: 18-22.

Qixiang, S., Guiying, W., Guoqing, Y., Qiang, M., Wenqi W. and Zhensheng, P. (2008). Influence of substitution of Sm, Gd, and Dy for La in $La_{0.7}Sr_{0.3}MnO_3$ on its magnetic and electric properties and strengthening effect on room-temperature CMR. J. Rare Earths. 26: 821-826.

Ling, L., Fan, J., Pi, L., Tan S. and Zhang, Y. (2008). Effect of magnetism and average radius at A-site on T_C in $Nd_{0.6}Ln_{0.1}Sr_{0.3}MnO_3$ (Ln = La, Pr, Gd, Dy) system. Solid State Comm. 145: 11-14.

Liang, Y.C., Zhong, H. and Liao, W.K. (2013). Nanoscale crystal imperfections-induced changes of characterization in manganite nanolayers with various crystallographic textures. Nanoscale Res. Letters. 8: 345-352.

❑❑❑❑❑